Computers and Fluids 228 (2021) 105069

Contents lists available at ScienceDirect

Computers and Fluids

journal homepage: www.elsevier.com/locate/compfluid

Stokes Eigenmodes on two-dimensional regular polygons

Pierre Lallemand [a], Lizhen Chen [a], Gérard Labrosse [a,b], Li–Shi Luo [a,c,*]

[a] Computational Science Research Center, Beijing 100193, China
[b] LAMPS (EA 4217 UPVD), Université de Perpignan, Perpignan, France
[c] Department of Mathematics & Statistics, Old Dominion University, Norfolk, VA 23529, USA

ARTICLE INFO

Keywords:
Stokes Eigenmodes on regular N-polygons and disc
Asymptotic behaviours of the Stokes Eigenmodes as the apex number $N \to \infty$
Lattice Boltzmann equation
Spectral element methods

ABSTRACT

The Stokes eigenmodes on two-dimensional regular polygons of N apexes, $3 \le N \le 40$, are studied numerically using two different solvers: the lattice Boltzmann equation and the Legendre–Galerkin spectral element method. In particular, the lowest 55 eigenmodes on regular N-polygons have been computed and investigated for the following properties including (a) symmetries, (b) the asymptotic behaviour of the Stokes eigenvalues $\lambda(N)$ in the limit of the apex number $N \to \infty$, *i.e.*, in the limit of a regular N-polygon becoming its circumcircle, (c) the splitting doublet modes due to boundary geometry of N-polygons, and (d) the one-to-one correspondence between the Stokes modes on regular N-polygons and on the disc.

1. Introduction

In our recent works [1–3], the Stokes eigenmodes on triangles [3], square [1], and cube [2] have been systematically studied by numerical means. The Stokes eigenmodes decay exponentially in time at rates that can be determined numerically. The structure of these eigenmodes has been analysed with the emphasis on their symmetry properties and multiplicity. In the present work, we will extend the previous analysis to two-dimensional regular polygons of N apexes on the circumcircle of unit radius. In particular, we will investigate the relationship between the Stokes eigenmodes on regular N-polygons and those on the disc and the effects of the boundary geometry of N-polygons on the eigenmodes.

It is worth noting that the Stokes eigenvalue problem on a domain Ω with some given boundary conditions, of either the Dirichlet or Neumann type, is of some general interest in mathematics. First of all, the Stokes eigenvalue problem is in fact closely connected to a more general problem — the Laplacian eigenvalue problem on the same domain Ω [4,5], which arises from various problems in mathematical physics. Ever since Kac [6] first raised the rhetorical question "*Can one hear the shape of a drum*?", the question has been raised and revised again and again [7–11]. There have also been a considerable effort to study the asymptotic behaviour of the eigenvalue of mth order elliptic operator, $\Delta^m := (\nabla \cdot \nabla)^m$, on a d-dimensional manifold [12–15] or even on a fractal domain Ω [16,17].

Secondly, from a more practical perspective, the study of Stokes problem has a significant implication on the computational fluid dynamics (CFD) in general. Many Navier–Stokes solvers are in fact Stokes solvers in essence, because the nonlinear convection term in the Navier–Stokes equation may be explicitly treated in time as a source term together with the momentum–diffusion part. It is interesting to note that this approach is effective even when the Reynolds number Re is very large. Thanks to the global nature of diffusion, the existence of small regions in the flow wherein the diffusion is dominant, mainly in the neighbourhood close to boundary, is sufficient to make the Stokes solvers to work effectively on the entire flow region.

It turns out that solving the Stokes problem is a nontrivial task, albeit it is a linear problem. For instance, it is challenging to properly evaluating the pressure field with the incompressibility constraint. To this end, a consistent spectral Stokes solver has been proposed [18], opening the way to an accurate determination of the Stokes eigenspace. This eigenspace has been determined on simple 2D domain, such as a square [1] and isosceles triangles [3]. And for the first time a linear correlation was established between the vorticity and the stream function in the core part of the domain, which reveals the periodic nature of the eigenmodes in the core region away from the no-slip domain boundary [1,3]. The Stokes eigenmodes on a 3D cube has also been investigated [19]. In the 3D case, numerically determining a significant number of eigenmodes even on a simple cubic domain seems to remain as a computational challenge to our computational capability. It is interesting to note that, there is no corner vortexes observed in the 3D case [20], as opposed to the 2D counterpart where there are corner vortexes.

We note that in the literature of the Stokes eigenmodes and related subjects, much effort has been focusing on the eigen-values of the

* Corresponding author.
E-mail addresses: pierre.lal@free.fr (P. Lallemand), lzchen@csrc.ac.cn (L. Chen), labrossenator@gmail.com (G. Labrosse), lluo@csrc.ac.cn, lluo@odu.edu (L.- Luo).

https://doi.org/10.1016/j.compfluid.2021.105069
Received 12 August 2020; Received in revised form 30 May 2021; Accepted 6 July 2021
Available online 15 July 2021

Stokes (or Laplacian) operator, very few work is about the eigenmodes and their properties, and the present work is devoted to the latter. The present work numerically investigates the asymptotic and symmetry properties of the Stokes eigenmodes on a regular polygon of N-apex in the limiting process of $N \to \infty$, *i.e.*, when the N-polygon morphs to a disc as the number of its apexes, N, increases. In particular, the relationship between the eigenmodes of an N-polygon and the disc defined by its circumscribed circle is the interested subject of this work. The remainder of this paper is organized as follows. Section 2 briefly states the eigenvalue problem associated with the Stokes equation and describes two numerical methods used to solve the Stokes eigenvalue problem — the lattice Boltzmann equation (LBE) and the Legendre–Galerkin spectral element method (LGSEM), Section 3 briefly reviews the solutions of the Stokes eigenvalue problem on the disc and their symmetry properties. Section 4 contains the main body of this work, based on the numerical results of the first 55 Stokes eigenmodes. The symmetry properties of the eigenmodes on regular N-polygons, the variation of the eigenvalues $\lambda(N)$ as the apex number N increases, the effect of the polygonal boundary on the eigenmodes, especially the splitting of doublets, and the correspondence between the Stokes modes on regular N-polygons and those on the disc. Finally, Section 5 summarizes our work and concludes the paper.

2. The Stokes equations and their numerical solvers

In what follows we will first describe the eigenvalues problem associated with Stokes equation in Section 2.1, and two different numerical methods used in this work, *i.e.*, the lattice Boltzmann equation and the Legendre–Galerkin spectral element method in Sections 2.2 and 2.3, respectively.

2.1. Stokes equation and its associated eigenvalue problem

We consider the following dimensionless, time-dependent Stokes equations for the primitive variables with initial and no-slip (Dirichlet) boundary conditions:

$$\partial_t \boldsymbol{u} = \Delta \boldsymbol{u} - \boldsymbol{\nabla} p, \quad \boldsymbol{\nabla}\cdot\boldsymbol{u} = 0, \qquad (\boldsymbol{r}, t) \in \Omega \times (0, T], \tag{1a}$$

$$\boldsymbol{u}(\boldsymbol{r}, t) = \boldsymbol{0}, \qquad \boldsymbol{r} \in \partial\Omega, \tag{1b}$$

$$\boldsymbol{u}(\boldsymbol{r}, t=0) = \boldsymbol{u}_0(\boldsymbol{r}), \qquad \boldsymbol{r} \in \Omega, \tag{1c}$$

where $\boldsymbol{u}(\boldsymbol{r}, t) := (u_x, u_y)$ is the flow velocity, $p(\boldsymbol{r}, t)$ is the pressure, and $\Delta := \boldsymbol{\nabla}\cdot\boldsymbol{\nabla} := \nabla^2$ is the Laplacian operator; $T > 0$, and Ω and $\partial\Omega$ are the flow domain and its boundary, respectively. If $\partial_t \boldsymbol{u} = -\lambda \boldsymbol{u}$, where $-\lambda$ is the algebraic temporal growth rate of $\boldsymbol{u}$, *viz.*, the Stokes eigenvalue, then the Stokes equations become the following eigen-system:

$$-\lambda \boldsymbol{u} = \Delta \boldsymbol{u} - \boldsymbol{\nabla} p, \quad \boldsymbol{\nabla}\cdot\boldsymbol{u} = 0, \qquad \boldsymbol{r} \in \Omega, \tag{2a}$$

$$\boldsymbol{u} = \boldsymbol{0}, \qquad \boldsymbol{r} \in \partial\Omega. \tag{2b}$$

In this work, we consider the above equations in two dimensions (2D), *i.e.*, $\boldsymbol{r} := (x, y)$.

The eigen-system (2) can be alternatively formulated with the vector-potential $\boldsymbol{A} := (0, 0, \psi)$, where $\psi := \psi(x, y)$ is the stream function in 2D. This leads to the following two-dimensional bi-harmonic system for $\psi(x, y)$ with the boundary conditions on ψ and $\partial\psi/\partial\hat{\boldsymbol{n}}$:

$$\Delta^2\psi = -\lambda\,\Delta\psi, \qquad \boldsymbol{r} \in \Omega, \tag{3a}$$

$$\psi = 0 = \frac{\partial\psi}{\partial\hat{\boldsymbol{n}}}, \qquad \boldsymbol{r} \in \partial\Omega, \tag{3b}$$

where $\hat{\boldsymbol{n}}$ is the unit vector out-normal to the flow boundary $\partial\Omega$. The Stokes eigenvalue problem on regular polygons of N apexes will be solved numerically with the techniques described next.

2.2. The lattice Boltzmann equation

The lattice Boltzmann equation (LBE, cf., *e.g.*, a recent review [21]) is one of the numerical technique used in this work to solve the Stokes equations. The LBE evolves on a uniform square Cartesian mesh of size $N_x \times N_y$ large enough to cover the flow domain Ω, with a discrete time $t_n = n\delta_t$, $n = 0, 1, 2, \ldots$. The specific lattice Boltzmann (LB) model used in this work has nine discrete velocities in 2D (D2Q9 model):

$$\begin{aligned} &\boldsymbol{c}_0 = (0, 0), \\ &\boldsymbol{c}_1 = (1, 0)c, \quad \boldsymbol{c}_2 = (0, 1)c, \quad \boldsymbol{c}_3 = (-1, 0)c, \quad \boldsymbol{c}_4 = (0, -1)c, \\ &\boldsymbol{c}_5 = (1, 1)c, \quad \boldsymbol{c}_6 = (-1, 1)c, \quad \boldsymbol{c}_7 = (-1, -1)c, \quad \boldsymbol{c}_8 = (1, -1)c, \end{aligned} \tag{4}$$

where $c := \delta_x/\delta_t$, and δ_x is the grid spacing of the Cartesian mesh. The variables in the LBE are the distribution functions $\{f_i(\boldsymbol{r}_j, t_n)\}$ corresponding to the discrete velocity set $\{\boldsymbol{c}_i\}$.

The LBE can be concisely written in the following vector form [22,23]:

$$\mathbf{f}(\boldsymbol{r}_j + c\delta_t, t_n + \delta_t) = \mathbf{f}(\boldsymbol{r}_j, t_n) - \mathbf{M}^{-1}\mathbf{S}\left[\mathbf{m}(\boldsymbol{r}_j, t_n) - \mathbf{m}^{(0)}(\boldsymbol{r}_j, t_n)\right], \tag{5}$$

where $\mathbf{m} := \mathbf{M}\mathbf{f}$ and $\mathbf{f} := \mathbf{M}^{-1}\mathbf{m}$,

$$\begin{aligned} &\mathbf{f}(\boldsymbol{r}_j + c\delta_t, t_n + \delta_t) := (f_0(\boldsymbol{r}_j, t_n + \delta_t),\ f_1(\boldsymbol{r}_j + \boldsymbol{c}_1\delta_t, t_n + \delta_t),\ \ldots, \\ &\quad f_8(\boldsymbol{r}_j + \boldsymbol{c}_8\delta_t, t_n + \delta_t))^\dagger, \\ &\mathbf{f}(\boldsymbol{r}_j, t_n) := (f_0(\boldsymbol{r}_j, t_n),\ f_1(\boldsymbol{r}_j, t_n),\ \ldots, f_8(\boldsymbol{r}_j, t_n))^\dagger, \\ &\mathbf{m}(\boldsymbol{r}_j, t_n) := (m_0(\boldsymbol{r}_j, t_n),\ m_1(\boldsymbol{r}_j, t_n),\ \ldots, m_8(\boldsymbol{r}_j, t_n))^\dagger, \\ &\mathbf{m}^{(0)}(\boldsymbol{r}_j, t_n) := (m_0^{(0)}(\boldsymbol{r}_j, t_n),\ m_1^{(0)}(\boldsymbol{r}_j, t_n),\ \ldots, m_8^{(0)}(\boldsymbol{r}_j, t_n))^\dagger, \end{aligned}$$

$\mathbf{S}$ is a diagonal matrix of relaxation rates to be given later, and $\mathbf{M}$ is the transform matrix which maps the distributions $\{f_i\}$ to the corresponding velocity moments $\{m_i\}$ and for the D2Q9 we use:

$$\mathbf{M} = \begin{pmatrix} 1 & 1 & 1 & 1 & 1 & 1 & 1 & 1 & 1 \\ 0 & 1 & 0 & -1 & 0 & 1 & -1 & -1 & 1 \\ 0 & 0 & 1 & 0 & -1 & 1 & 1 & -1 & -1 \\ 0 & 1 & -1 & 1 & -1 & 0 & 0 & 0 & 0 \\ 0 & 0 & 0 & 0 & 0 & 1 & -1 & 1 & -1 \\ -4 & -1 & -1 & -1 & -1 & 2 & 2 & 2 & 2 \\ 0 & -2 & 0 & 2 & 0 & 1 & -1 & -1 & 1 \\ 0 & 0 & -2 & 0 & 2 & 1 & 1 & -1 & -1 \\ 4 & -2 & -2 & -2 & -2 & 1 & 1 & 1 & 1 \end{pmatrix}.$$

With the transform matrix $\mathbf{M}$ defined above, the zeroth-order $m_0 = \rho$ is the mass density; the first-order moments $m_1 := \rho u_x$ and $m_2 = \rho u_y$ are the x and y component of the flow momentum $\rho\boldsymbol{u}$, respectively, where $\boldsymbol{u} := (u_x, u_y)$ is the flow velocity; $m_3 := p_{xx}$ and $m_4 := p_{xy}$ are second-order moments related to the components of the stress tensor; $m_5 := e$ is related to energy; $m_6 := q_x$ and $m_7 := q_y$ are related to the x and y component of energy flux, respectively; and $m_8 := \varepsilon$ is a fourth-order moment.

The mass density and the flow momentum are the only conserved moments in the LB system, and they are obtained from the distribution functions $\{f_i\}$ as the following:

$$\rho = \textstyle\sum_i f_i, \qquad \rho\boldsymbol{u} = \textstyle\sum_i f_i \boldsymbol{c}_i. \tag{6}$$

For the Stokes equations, the equilibria of the non-conserved moments are:

$$m_3^{(0)} := p_{xx}^{(0)} = 0, \qquad m_4^{(0)} := p_{xy}^{(0)} = 0, \qquad m_5^{(0)} := e^{(0)} = -2\rho, \tag{7a}$$

$$m_{6,7}^{(0)} := q_{x,y}^{(0)} = -\rho u_{x,y}, \tag{7b}$$

$$m_8^{(0)} := \varepsilon^{(0)} = \rho. \tag{7c}$$

Of course, the equilibria of the conserved moments are equal to themselves.

With the given ordering of the moments according to the rows of $\mathbf{M}$, the relaxation rates are given by

$$\mathbf{S} := \mathrm{diag}(s_0, s_1, \ldots, s_8) = \mathrm{diag}(1, 1, 1, s_\nu, s_\nu, s_e, s_q, s_q, s_\varepsilon), \tag{8}$$

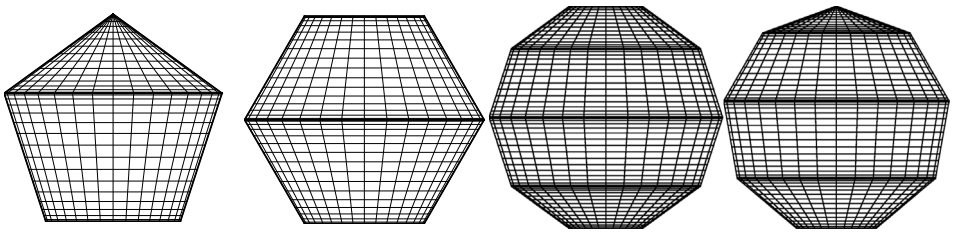

Fig. 1. From left to right, the grids for a regular pentagon, hexagon, decagon, and nonagon, with a 17 × 17 mesh for each quadrangular and triangular sub-domain.

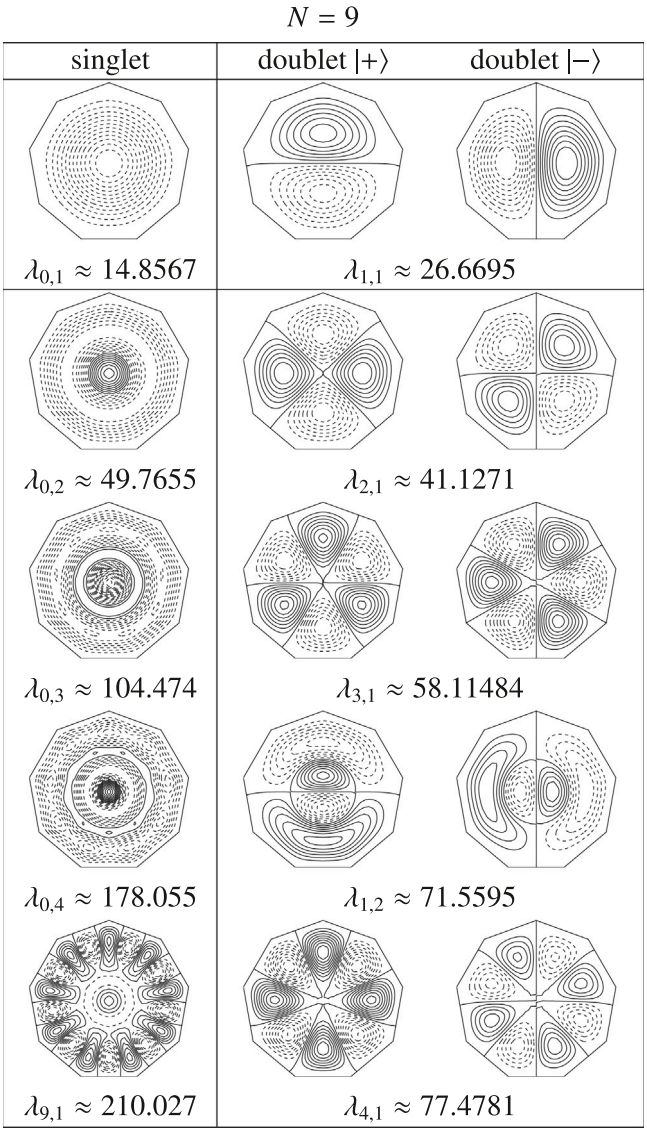

Fig. 2. The first five Stokes eigenmodes in each symmetry family of the nonagon. The contours of the stream function $\psi_{mn}(x, y)$. The solid and dashed lines indicate positive and negative values of ψ, respectively. The eigenfunctions are computed with LGSEM.

where $s_e = 0.9$ and $s_\varepsilon = 1.3$ unless otherwise specified, and

$$\frac{1}{s_\nu} - \frac{1}{2} = \frac{1}{2\sqrt{3}}, \quad \frac{1}{s_q} - \frac{1}{2} = \frac{1}{\sqrt{3}}, \quad \left(\frac{1}{s_\nu} - \frac{1}{2}\right)\left(\frac{1}{s_q} - \frac{1}{2}\right) = \frac{1}{6}. \tag{9}$$

The shear viscosity in the LBE is determined by the relaxation rate s_ν as the following:

$$\nu = \frac{1}{3}\left(\frac{1}{s_\nu} - \frac{1}{2}\right) = \frac{1}{6\sqrt{3}}. \tag{10}$$

It can be shown that ρ and $\boldsymbol{u}$ obey the Navier–Stokes equations for near incompressible athermal flows, and the LBE is a second-order scheme for the velocity $\boldsymbol{u}$ [24–28].

With the relaxation rates s_ν and s_q satisfying the above relationship (9), the damping constant of shear waves can achieve fourth-order accuracy [29,30], and this enhanced accuracy would be needed to separate close eigenvalues, which will be discussed later. The no-slip boundary conditions can be realized by the simple bounce-back scheme provided that the relaxation rates s_ν and s_q satisfy the relationship (9). For an arbitrary curved boundary which is not a straight line exactly aligned with a lattice line, its position is defined by its intersections with the lattice lines of the mesh, and interpolations are used to approximate the geometry of the boundary [31]. In this work, quadratic interpolations are used in the boundary conditions [31]. Because of the interpolations, the mass in the LBE is no longer conserved exactly; consequently the eigenvalue corresponding to the mass conservation is not exactly equal to 1. The LBE will be used to solve indirectly the Stokes equations for the primitive variables $\boldsymbol{u}$ and p, *i.e.*, Eqs. (2).

For the Stokes flows with appropriate boundary conditions on a domain Ω discretized by N_{LB} points, the lattice Boltzmann system (5) can be written as the following linear system:

$$\mathbf{F}_n = \mathbf{A}^n \mathbf{F}_0, \quad \mathbf{F}_n := \mathbf{F}(t_n), \quad \mathbf{F}_0 := \mathbf{F}(t_0), \tag{11}$$

where $\mathbf{F}$ denotes the vector of $9N_{\mathrm{LB}}$ dimensions for the D2Q9 model, and $\mathbf{A}$ denotes the matrix of size $(9N_{\mathrm{LB}})^2$ which can be easily derived from the LB system (5). Thus the Stokes eigenvalues are in fact those of the matrix $\mathbf{A}$ and the flow fields $\rho(x, y)$ and $\boldsymbol{u}(x, y)$ can be directly obtained from the eigenvectors of $\mathbf{A}$ through (6).

When the flow domain Ω is discretized with a large number of nodes, $\mathbf{A}$ is a very large but sparse matrix and its eigenvalues are computed using the Arnoldi algorithm, which only requires the data of one iteration $\mathbf{F}_n \to \mathbf{F}_{n+1}$. For the sake of computational efficiency, instead of $\mathbf{A}$, we compute the eigenvalues of $\mathbf{B} := \mathbf{A}^{2k+1}$ with, *e.g.*, $15 \le k \le 25$ [27].

The Arnoldi algorithm is adapted from the sample code dndrv1.f in ARPACK library, in which the matrix–vector routine av.f is replaced by the LBE scheme $\mathbf{F}_1 = \mathbf{A}\mathbf{F}_0$. The components of the initial state $\mathbf{F}_0$, *i.e.*, the initial values of the distribution functions $\{f_i(t_0)\}$, are uniform random numbers in the interval $[-1, +1]$.

The Stokes eigenvalue λ is directly computed from a (complex) eigenvalue of $\mathbf{A}$, ζ, as the following:

$$\lambda = -\mathrm{Re}(\ln \zeta)\frac{L^2}{\nu}, \tag{12}$$

where L is a characteristic length specific to the problem. The error tolerance on the Stokes eigenvalues is 10^{-9}, which is also the stopping criterion for a calculation. This approach has been validated previously [2,19]. While the Stokes eigenvalues can be computed by the LBE rather accurately, it should be noted that the flow fields obtained with the LBE are by no means as accurate, due to its low-order spatial accuracy.

2.3. Legendre-Galerkin spectral element method

The Legendre–Galerkin spectral element method (LGSEM) is the second technique used to solve the Stokes eigenvalue problem (3) on a regular polygon in 2D. A regular polygon is decomposed into symmetric quadrangular domains when the number of apexes N is even, and with one additional symmetric triangular domain when it is odd, and both quadrangular and triangular domains are mapped into a unit square. The unit square is then discretized with uniform mesh of $N_S \times N_S$ points in the mapped coordinate system. As an example, the meshes of size 17×17 on a quadrangular or triangular domain decomposed for regular pentagon, hexagon, decagon, and nonagon are illustrated in Fig. 1.

With the Duffy mapping [32], a triangle is mapped into a unit square, on which the eigen-problem is solved [33–37]. The mapping transforms each differential operator of the problem into a combination of mixed partial-derivative operators multiplied by a function of the new coordinates [38,39].

The LGSEM solver is based on the stream-function formulation (3) discretized by a Legendre–Galerkin method. The basis functions are tensorial products of appropriate 3-term linear combination of Legendre polynomials on a square [40]. The details of constructing the matrices to compute the Stokes eigenvalues λ are given in our previous work (cf., *e.g.*, [3]). Once the matrices are constructed, the subroutine dggev in LAPACK is used to compute the eigenmodes. Calculations with different mesh size N_S (in one dimension) have been conducted to ensure the numerical results are indeed mesh-size independent. We note that the eigenvalues obtained with $N_S = 42$ already have attained the precision of 10 digits, and the results we present in what follows are obtained with $N_S = 82$ unless otherwise stated.

To compare the eigenvalues obtained by both the LBE and LGSEM with those on the disc of radius R, proper normalization has to be done. For LGSEM and disc, $\nu = 1$ and $R = 1$. For LBE, ν is given by Eq. (10) and R is typically about 100 in the lattice units of $\delta_x = \delta_t = 1$, therefore the normalization of Eq. (12) must be considered. It has been shown [3] that the eigenvalues are approximately in proportion to the inverse of the area of the flow domain, $|\Omega|^{-1}$. To eliminate this area-dependence, the computed eigenvalue λ_* should be further normalized as the following:

$$\lambda = \lambda_* \frac{A_N}{A_\infty} = \lambda_* \frac{\sin(2\pi/N)N}{2\pi}, \tag{13}$$

where $A_N = \sin(2\pi/N)NR^2/2$ is the area of the N-polygon with the circumcircle of radius R and $A_\infty = \pi R^2$ is the area in the circumcircle.

The computational complexity of the LGSEM is $O(M^3) = O(K^6)$, where M and K are the total number of collocation points, which is also the dimension of the matrix to be solved, and the number of points in each dimension, respectively, while the computational complexity of the LBE method is $O(N_{LB}^3)$, where N_{LB} is the total number of grid points in fluid domain, although the complexity of LBE flow solver is only $O(N_{LB})$.

The reason this work employs two numerical methods, *i.e.*, the LBE and LGSEM is the following. While the LBE, an iterative method with a second-order spatial accuracy, is very effective and efficient to compute the eigenmodes, in contrast, the LGSEM, a high-order direct method, can yield much more accurate results for both the eigen-functions and eigen-values. As shall be demonstrated later, sometimes the difference between two distinctive eigen-values are so small that we must use the LGSEM to resolve the difference. Therefore, in our computations the LBE is used first to obtain the eigenmodes, then the LGSEM is used to ascertain the accuracy of the results when necessary. Both codes based on the LBE and LGSEM codes were written by the authors, and they have been tested thoroughly and independently and cross-validated previously [2,3,19].

3. Stokes modes on a unit disc

The eigenvalues problem (3) on the disc of unit radius can be solved analytically. With the polar coordinates (r, θ), the solution of (3) is given in terms of the Bessel function of the first kind of order m, J_m, *viz.*,

$$\psi_{mn}(r, \theta) = \left[J_m(\sqrt{\lambda_{mn}})r^m - J_m(\sqrt{\lambda_{mn}}r)\right] \times \begin{cases} \cos(m\theta), \\ \sin(m\theta), \end{cases} \tag{14}$$

where $-\lambda_{mn}$ is the eigenvalue, and m and n are the angular and the radial *quantum* numbers, respectively. For $m > 0$ there are two distinct eigenmodes with the same eigenvalue. There are two boundary conditions on ψ at $r = 1$:

$$\psi_{mn}(r = 1, \theta) = 0 \quad \text{and} \quad \frac{\partial \psi_{mn}(r = 1, \theta)}{\partial r} = 0,$$

and $\partial\psi_{mn}(r = 1, \theta)/\partial r = 0$ leads to

$$J_{m+1}(\sqrt{\lambda_{mn}}) = 0.$$

The solution (14) shows that the eigenmodes appear either alone with $m = 0$ or in pairs with $m > 0$, corresponding to a set of singlets or a set of doublets, respectively. There is thus an infinite number of modes for each given m. On the disc, the solution $\psi_{mn}(r, \theta)$ has $n - 1$ zeros along r direction, thus $n \geq 1$. The smallest value of λ_{mn} is

$$\lambda_{01} = 14.681971\ldots,$$

which is the square of the first root of $J_1(r) = 0$, and it corresponds to the first singlet — the most fundamental Stokes mode on the disc.

The symmetry of the Stokes eigenmodes on the unit disc resides in the angular part of $\psi_{mn}(r, \theta)$, *i.e.*, $\cos(m\theta)$ and $\sin(m\theta)$; they have the symmetry of dihedral groups D_m, which consist of the cyclic groups C_m and reflections about m axes. Specifically, the singlets ($m = 0$) are independent of θ, therefore are invariant under any θ-rotation about the centre of the disc. Each doublet mode (m, n) with $m > 0$ consists of two *physically* identical modes which are related to each other by a rigid-body rotation of $\pi/2m$, denoted as R_m, because $\cos[m(\theta+\pi/2m)] = -\sin(m\theta)$ and $\sin[m(\theta + \pi/2m)] = \cos(m\theta)$. Also, each member of a doublet mode (m, n) is invariant under the $2\pi/m$-rotation or m-fold symmetry, *i.e.*, C_m.

In addition, the eigenmodes enjoy the symmetry S with respect to the diameters with the angle $\theta = 2k\pi/m$, $0 \leq k \leq (m - 1)$. The modes of $\cos m\theta$ are symmetric whereas the modes of $\sin m\theta$ are anti-symmetric with respect to these diameters, and they are denoted respectively as $|+\rangle$ and $|-\rangle$.

4. The results and discussions

This section presents our numerical results of the Stokes eigenmodes on two-dimensional regular N-polygons for $3 \leq N \leq 40$. In particular, Section 4.1 discusses the symmetry properties of the eigenmodes on regular N-polygons and shows the first few modes on nonagon ($N = 9$) and decagon ($N = 10$) to illustrate different behaviours depending on the parity of N. Section 4.2 studies the variation of the eigenmodes as a function of N, and the asymptotic behaviours of the eigenvalues $\lambda(N)$ in the limit of $N \to \infty$. Section 4.3 investigates the mechanism responsible for doublet splitting due to boundary geometry of an N-polygon. Section 4.4 studies the one-to-one correspondence between the eigenmodes on an N-polygon and those on the disc.

4.1. The symmetry properties of the eigenmodes

To demonstrate some qualitative properties of Stokes eigenmodes on regular polygons, the contours of the stream function $\psi(x, y)$ for the first five modes in each symmetry family for the nonagon and decagon are shown in Figs. 2 and 3, respectively. All modes can be classified as either singlet or doublet. All modes on regular N-polygons can be

characterized by the pair of quantum number (m, n) for the eigenmodes on a disc (cf. the pertaining discussion in Section 3). Certainly, the eigenmodes on an N-polygon differ from those on a disc, however, their qualitative properties allow them to be characterized by the quantum numbers (m, n).

First of all, the structural similarities between the polygon and disc modes can be observed. For instance, the mode with $\lambda_{0,4} \approx 178.05$ on the nonagon can be seen as the disc mode (0, 4) with a small admixture of the mode (9, 1). Because this mode is dominated by the disc mode (0, 4), hence it is labelled as mode (0, 4). These singlet modes have a one-to-one correspondence with disc modes.

The geometry of a polygon certainly dictates symmetry of the eigenmodes. A regular polygon of N apexes has either N or $2N$ geometrical centre-lines or symmetric axes for odd N and even N, respectively. The symmetry about these axes is respected by the eigenmodes. For a regular polygon with odd-number apexes, the symmetric axes go through the centre and an apex. However, for a regular polygon with even-number apexes, there are two sets of symmetric axes: one going through the centre and two opposite apexes, and the other bisect two opposite arcs. In the coordinate system used here, for a odd-apex-number polygon, the y axis is the symmetric axis, and for an even-apex-number polygon, the x axis is the long symmetric axis, *i.e.*, two opposite apexes reside on it, while the y axis is the short symmetric axis (cf. Fig. 1). The $\cos m\theta$ parts of the doublets are symmetric about the axes, while the $\sin m\theta$ parts are anti-symmetric, and they will be denoted respectively by $|+\rangle$ and $|-\rangle$.

Among the 55 studied modes, two seem to be ambiguous as how they should be labelled by the quantum numbers, *i.e.*, the mode of $\lambda \approx 210.027$ on the nonagon in Fig. 2 and the one of $\lambda \approx 241.908$ on the decagon in Fig. 3. The mode on nonagon is similar to the disc doublet (9, 1) near the boundary, superposed with the disc singlet (0, 2) in the core region. The same can be observed for the decagon mode of $\lambda \approx 241.908$, it is a mixture of disc doublet (10, 1) around its edge and singlet (0, 2) at its core. Pictorially, these modes have an $m = 0$ core surrounded by a $m > 0$ peripheral. As will be discussed later in Section 4.3, these modes are the members of the pairs due to the splitting of doublets, therefore, it is no longer unique to label these modes with the pair of quantum numbers (m, n) alone, there is a two-to-one correspondence with disc modes, that is, two polygon singlets correspond to one disc doublet in this case. However, these modes can be distinguished uniquely with additional symmetry information, which will be discussed later.

4.2. From polygons to disc

Geometrically, a disc can be seen as the limiting case of regular N polygons, as N goes to infinity. In what follows, we will study the behaviour of the eigenvalues on N-polygons as $N \to \infty$. To this end, we compute the eigenvalue $\lambda(N)$ on polygons with N apexes for $N \le 40$. The calculation of the eigenvalues is carried out by means of the LBE, validated by the LGSEM solver whenever necessary (cf. Section 2.3). For example, in the pentagon ($N = 5$), the difference between two eigenvalues, $\lambda_{1,4} \approx 217.343474$ and $\lambda_{9,1} \approx 217.287665$, resides in the fourth significant digit. It requires accurate numerics to distinguish two very close eigenvalues definitively. The LGSEM solver proves to be particularly useful in this case, for it can ensure the accuracy of more than ten significant digits. While the LB algorithm (with the parameters of Eq. (9)) can detect this small difference in λ, although not accurately, it can, nevertheless, capture the spatial structures of both eigenmodes very well.

The first 55 eigenvalues $\lambda(N)$ computed by the LBE are shown in Fig. 4, from which the following observations can be made:

1. All singlets remain singlets for any N polygons.
2. Most doublets remain as doublets, except a few which split to become two singlets, at given N, for $m = N/2$ or $m = N$. This doublet splitting is a consequence due to the matching between the angular component of a mode and the boundary geometry (cf. detailed discussion in Section 4.3).
3. The eigenvalues $\lambda_{mn}(N)$ for the singlets generated by split doublets fall on a family of parabola-like curves $\lambda(N) \approx c_0 + c_1 N^{\alpha}$ with $\alpha \approx 3/2$.
4. For $N > 10$, the first 18 area-normalized eigenvalues $\lambda_{mn}(N)$ decrease monotonically as N increases, and converge to the corresponding eigenvalues λ^{∞}_{nm} on the disc as $N \to \infty$:

$$\lambda_{mn}(N) = \lambda^{\infty}_{nm} + a\, N^{-\beta}, \quad a > 0, \quad 2.30 < \beta < 2.75.$$

To illustrate how the Stokes eigenmodes evolve as N increases, Fig. 5 shows two sets of modes, namely, the modes of (5, 1) and (10, 1), with $N = 9$, 10, 12, and on the disc ($N = \infty$). The contours of the stream-function $\psi_{m,n}(x, y)$ and the eigenvalues $\lambda_{m,n}(N)$ are included in the figure. For doublets, only one member of eigenmodes is shown. The super-script "S" and "D" correspond to singlet and doublet, respectively. It can be seen that a singlet pair generated from a doublet splitting consists of a symmetric state $|+\rangle$ and an anti-symmetric $|-\rangle$, and this information is included in the super-script, whenever appropriate, to make labelling unique. Two pairs of singlets generated by two split doublets are shown in Fig. 5, the first pair, $\lambda^{S|-\rangle}_{5,1}$ and $\lambda^{S|+\rangle}_{5,1}$, comes from the doublet $\lambda_{5,1}$, with $m = 5 = 10/2 = N/2$, and the second comes from $\lambda_{10,1}$, with $m = 10 = N$. By comparing these two pairs of modes with the corresponding modes on the disc, it is easy to see the similarity of the modes in the peripheral region adjacent to the boundary, as well as the differences in the core region. The mechanism of the doublet splitting will be discussed next in Section 4.3.

4.3. Mode-splitting and geometry matching

Observation on the Stokes modes on regular N polygons suggests that lifting the degeneracy of a doublet mode is possible when m, the angular quantum number of the mode, is related to N, the number of apexes of the polygon, in a certain way. To investigate the mechanism responsible for the lifting, we study the effect of a sinusoidal perturbation on the radial coordinate of the boundary in the following form:

$$r(\theta) = 1 + h\, \cos(q\,\theta), \quad h \ll 1. \tag{15}$$

We compute the Stokes eigenmodes on the disc with wavy boundary by using the LB solver. The computed Stokes modes are identified with their angular and radial quantum numbers, (m, n), as well as their multiplicities, *i.e.*, the modes are either singlets or doublets.

We select the case of $q = 8$ and study the effect of the perturbation magnitude h on the Stokes modes on the disc with the wavy boundary. We study the first nine modes on the unperturbed, perfect disc, *i.e.*, $h = 0$. These nine modes are: (0, 1), (0, 2), (4, 1), (0, 3), (4, 2), (0, 4), (8, 1), (4, 3), and (0, 5), listed in successively increase of the eigenvalue $\lambda_{m,n}$. Among them, five are doublets ($m > 0$), *i.e.*, (4, 1), (4, 2), (8, 1), and (4, 3). When the boundary is subject to the perturbation of $h\cos(8\theta)$, all four doublets are split to be four pairs of singlets, whereas all five singlets remain as singlets, as shown in Fig. 6. For all four doublets, it is either $m = 4 = q/2$ or $m = 8 = q$ ($q = 8$). It can also be seen from Fig. 6 that the difference between the eigenvalues of two singlets in a pair split from a doublet monotonically grows as the magnitude of perturbation h increases in the range of $0 < h \le 0.03$. The consequence of the splitting doublets is that, on a regular octagon, the first nine eigenmodes on the disc become thirteen modes: four doublets split into eight singlets, and the other five genuine singlets remain as singlets.

With the same procedure using the LB solver, as for the case of $q = 8$, we have also studied all the cases with the wave number of the perturbation $3 \le q \le 16$ and compiled in Table 1 all the doublets, indicated by their quantum numbers (m, n), which split into pairs of

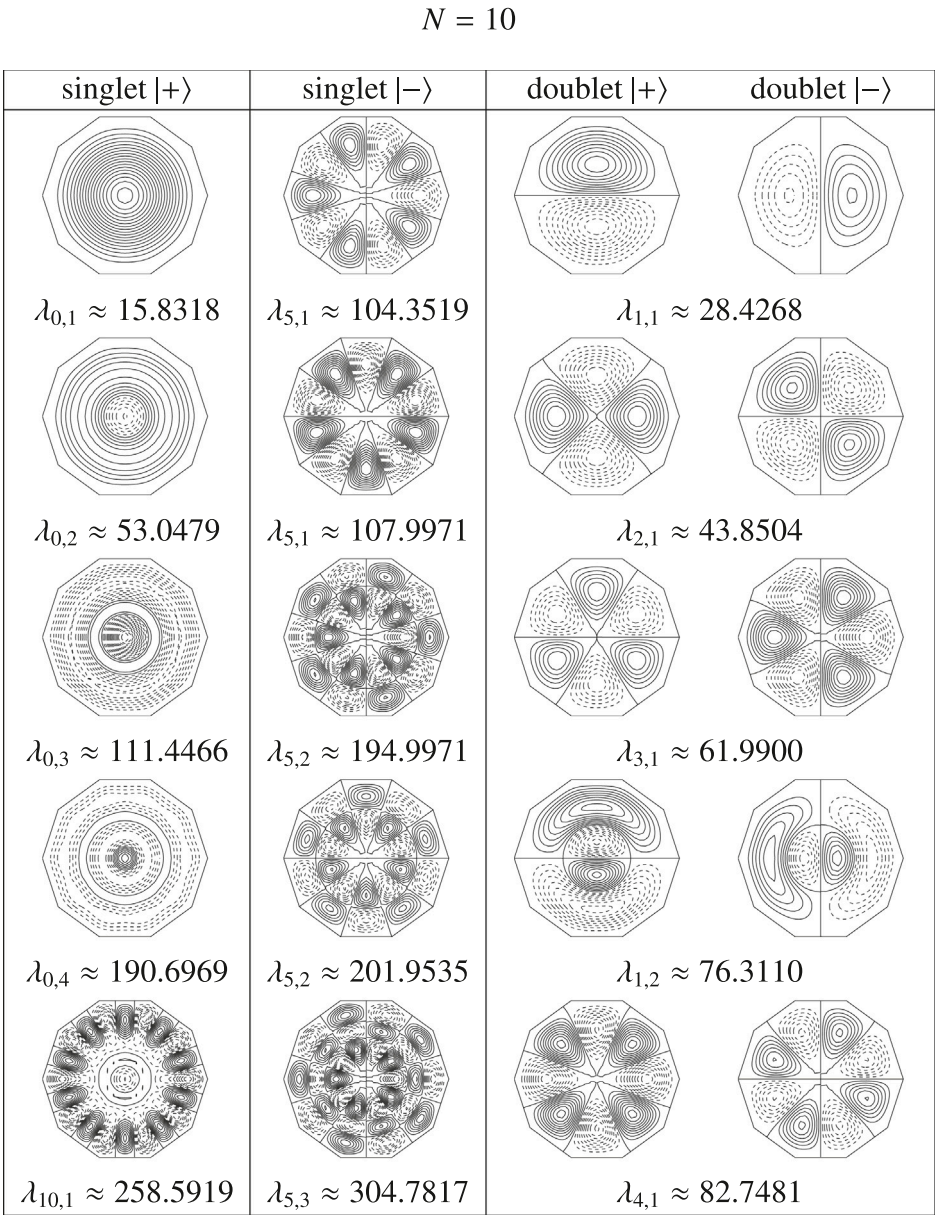

Fig. 3. The first five Stokes eigenmodes in each symmetry family of the decagon. Similar to Fig. 2.

singlets on the disc with the sinusoidal boundary. All the pairs of singlets in Table 1 are indicated by pairs of △ and ▽ in Fig. 4. This result demonstrates the fact that, for the splitting states, the angular quantum number m is a multiple of either $N/2$ for an even N or N for an odd N, that is, the boundary geometry of a regular N-polygon preferentially accommodates those eigenmodes whose angular parts "resonate" or "fit" with the boundary geometrically. It can be seen that the information of the states shown in Fig. 6 is consistent with that shown in Fig. 4 and Table 1 corresponding to the case of octagon ($N = 8$).

4.4. Correspondence between N-polygon and disc modes

We now study the connection between the Stokes eigenmodes in an N polygon and those in the disc. Table 2 tabulates the number of singlets and doublets for the first 55 modes in regular N polygons for $3 \le N \le 22$, as well as in the disc. It can be seen that the number of singlets (and thereby that of doublets) is the sum of the singlets on the disc and the singlets born from the splitting doublets, which are listed

Table 1
The doublet Stokes eigenmodes on the disc which will split into two singlets when the disc boundary is subjected to a sinusoidal perturbation, *i.e.*, $r(\theta) = 1 + h\cos(q\theta)$, with $h \ll 1$.

q	Splitting doublet modes
3	(3, 1), (3, 2), (6, 1), (3, 3), (9, 1), (6, 2)
4	(2, 1), (4, 1), (2, 2), (6, 1), (4, 2), (2, 3), (8, 1), (6, 2), (10, 1), (4, 3), (2, 4)
5	(5, 1), (5, 2), (5, 3)
6	(3, 1), (3, 2), (6, 1), (3, 3), (6, 2), (9, 1)
7	(7, 1), (7, 2)
8	(4, 1), (4, 2), (8, 1), (4, 3), (8, 2)
9	(9, 1)
10	(5, 1), (5, 2), (10, 1), (5, 3)
11	(11, 1)
12	(6, 1), (6, 2)
13	
14	(7, 1), (7, 2)
15	
16	(8, 1), (8, 2)

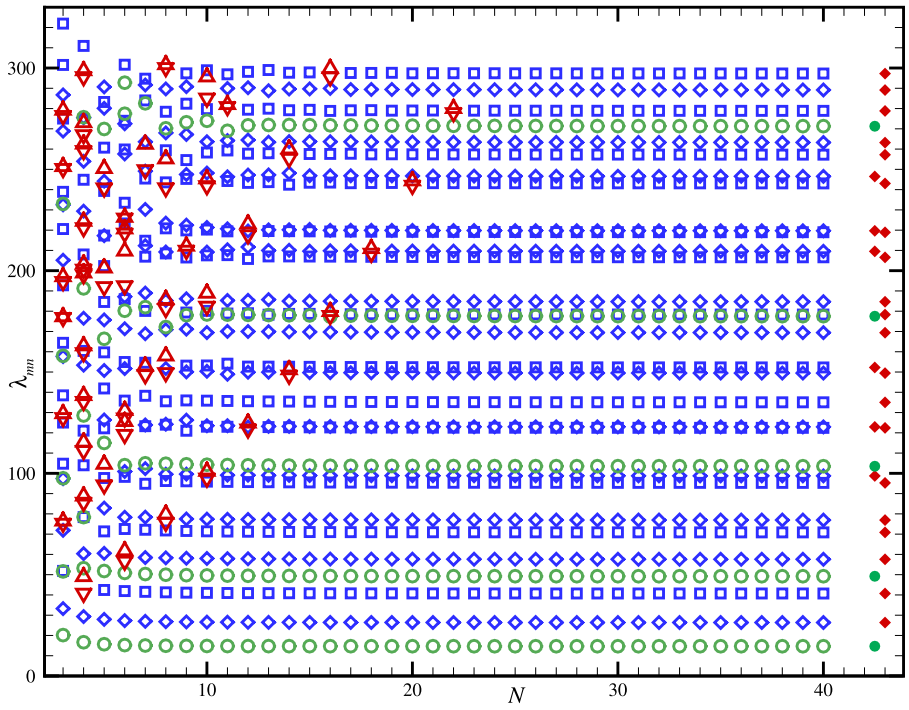

Fig. 4. The Stokes eigenvalues $\lambda_{mn}(N)$ on regular N-polygons obtained the LBE (cf. Eq. (13)). The singles are indicated by circles (○), and the doublets are represented by diamonds (◇) or squares (□). Triangles (△) and inverse triangles (▽) represent the pairs of singlets due to splitting of doublets. The solid bullets (•) and diamonds (◆) are the singlets and doublets on the disc ($N = \infty$), respectively. For $3 \le N \le 6$ and $N \ge 7$, 55 and 57 states are shown, respectively.

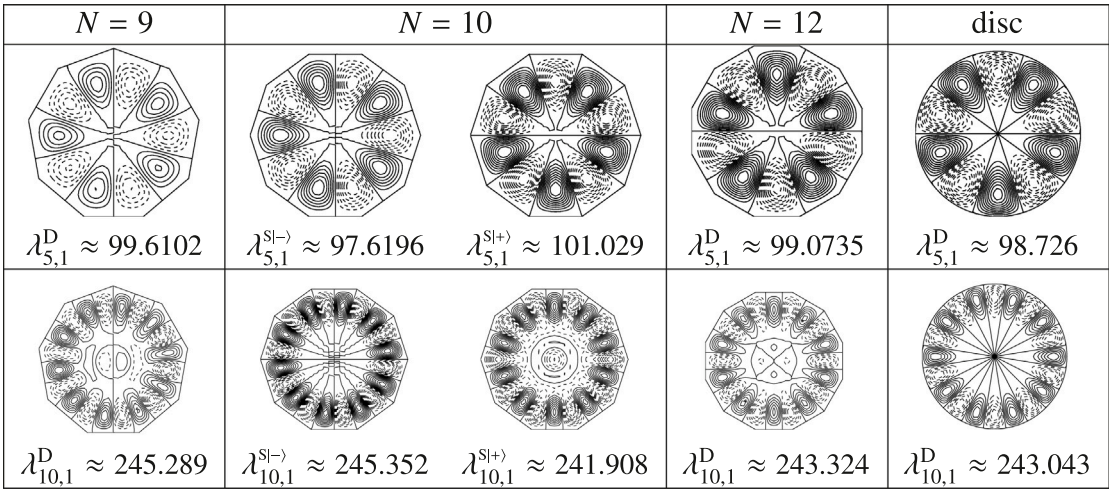

Fig. 5. The contours of the stream-function $\psi_{n,m}(x, y)$ corresponding to the eigenmodes (5, 1) and (10, 1) with $N = 9$, 10, and 12. The corresponding modes on the disc are also shown in the last row. This shows the evolution of modes as N increases, and the singlets generated from doublet splitting on the decagon ($N = 10$).

in Table 1 (which includes the doublet (8, 2) for $N = 16$ beyond the first 55 modes). There is a one-to-one correspondence between the Stokes eigenmodes on a regular N-polygon and those on the disc. For the disc singlets with zero angular quantum number m, they remain as singlets on the polygons. Therefore they are uniquely labelled by their quantum numbers $(0, n)$, for any n.

There is a second category of singlets, which are the results of splitting doublets on the disc. These singlets appear in pairs, each pair corresponds to a doublet, and the singlets in each pair correspond to the doublets of the same symmetry, thus they are labelled by their symmetries, in addition to their quantum numbers (m, n) and multiplicity. The way the splitting doublets appear is also interesting. In the notation $[N](m, n)$ for a state on a regular N-polygon, the first and second series of splitting doublets include those with $m = N/2$ for even $N \ge 3$, and $n = 1$ and 2, respectively:

$[4](2, 1), [6](3, 1), [8](4, 1), \ldots, [2m](m, 1), \ldots,$

$[4](2, 2), [6](3, 2), [8](4, 2), \ldots, [2m](m, 2), \ldots,$

and the third one includes the doublets with $m = N$, for all $N \ge 3$, and $n = 1$:

$[3](3, 1), [4](4, 1), [5](5, 1), \ldots, [m](m, 1), \ldots.$

Lastly, there are remaining doublets on N-polygons, which have a one-to-one correspondence to their doublet counterparts on the disc. Therefore, with a given N, all eigenmodes are uniquely labelled by the pair of quantum numbers (m, n), the multiplicity, and the symmetries. Consequently, all the eigenmodes on a regular N-polygon have a one-to-one correspondence to those on the disc.

Table 2
The number of singlets and doublets in the first 55 Stokes eigenmodes in regular N-polygons for $3 \le N \le 22$ and the disc.

Mode	N																				
	3	4	5	6	7	8	9	10	11	12	13	14	15	16	17	18	19	20	21	22	Disc
Singlet	17	27	11	17	9	13	7	13	7	9	5	9	5	7	5	7	5	7	5	7	5
Doublet	38	28	44	38	46	42	48	42	48	46	50	46	50	48	50	48	50	48	50	48	50

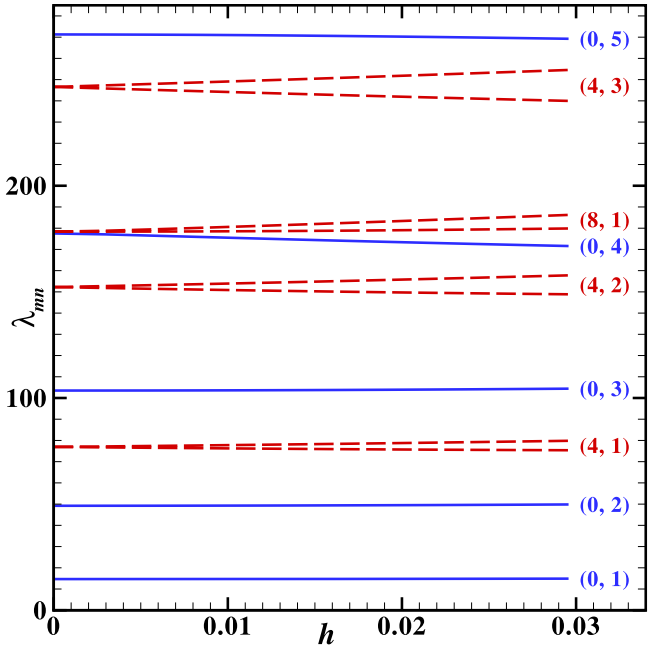

Fig. 6. The dependence of $\lambda_{mn}(h)$ on the perturbation amplitude h, for the first nine Stokes eigenvalues λ_{mn} on the disc with the sinusoidal perturbation $h\cos(8\theta)$ on its boundary. The solid and dashed lines represent singlet ($m = 0$) and doublet ($m > 0$) modes on the unperturbed disc ($h = 0$).

5. Conclusions and summary

In this work we solve the Stokes eigenvalue problem on regular N-polygons in 2D with two drastically different numerical methods: the lattice Boltzmann method and the Legendre–Galerkin spectral element method; the former is second-order accurate, while the latter is spectrally accurate. The LB method is an efficient method which allows us to carry out numerical calculations speedily. Our numerical results were obtained with the LB method, validated with the LGSEM whenever necessary. We present the first 55 eigenmodes on regular N-polygons with $3 \le N \le 40$.

Our main objective is to study the Stokes eigenmodes on regular N-polygons and their relationships with the eigenmodes on the circum-disc. Our main results can be summarized as follows. We first observe the effect of the boundary geometry on the Stokes eigenmodes. We note that all the Stokes eigenmodes on an N-polygon have an one-to-one correspondence with those on the circum-disc. The main effect of the boundary geometry is on Stokes eigenvalues: compared to their counterparts on the disc, the eigenvalues for most eigenmodes on an N-polygon are increased (by at least the ratio of the area of the circum-disc to that of the polygon), and especially so for small N's. As N increases, all eigenvalues monotonically and smoothly decrease to their counterparts on the disc.

A second observation is that a doublet mode may split due to the boundary geometry of an N-polygon, *i.e.*, the boundary geometry of an N-polygon may lift the degeneracy of some doublets. This splitting of doublets to two singlets occurs more often with small N. Also, as N increases, the occurrence of the splitting takes place in higher and higher order modes. In fact, the eigenvalues of the splitting modes, $\lambda(N)$, can be fitted by a family of concave curves.

Finally, we can make the following conclusion regarding the nature of the Stokes eigenmodes on regular N-polygons. Because each eigenmode on an N-polygon has an unique counterpart on the disc and all the eigenmodes on regular N-polygons converge smoothly to their counterparts on the disc as N increases — the irregularities occur only in small N's ($N \le 7$), as indicated in Fig. 4, therefore, there is no qualitative difference between the eigenmodes on regular N-polygons and their counterparts on the disc for the most part, and the differences are mostly quantitative, such as the values of the eigenvalues and eigenfunctions. In other words, the eigenmodes adapt to the boundary geometry of N-polygons without fundamentally changing their qualitative properties, such as the symmetries.

Nomenclatures

Alphabetical symbols and acronyms:

- A_N: the area of an N-polygon, *i.e.*, $A_N := NR^2\sin(2\pi/N)/2$
- A_∞: the area of the circumcircle of an N-polygon, *i.e.*, $A_\infty := \pi R^2$
- $\boldsymbol{A}$: the vector potential
- $\mathbf{A}$: the LBE evolution operator of the size $(QN_{\mathrm{LB}})^2$, *i.e.*, $\mathbf{F}_{n+1} = \mathbf{A}\mathbf{F}_n$
- $\mathbf{B} := \mathbf{A}^{2k+1}$
- c: the lattice velocity, *i.e.*, $c := \delta_x/\delta_t$
- $\boldsymbol{c}_i$: the ith discrete velocity in the LBE
- $e = m_5$ the second-order moment related to energy
- $\mathbf{F}_n$: a state vector of the size QN_{LB} in the LBE at t_n
- $f_i(\boldsymbol{r}_j, t_n)$: the mass distribution function corresponding to $\boldsymbol{c}_i$
- $\mathbf{f}(\boldsymbol{r}_j, t_n) := (f_0, f_1, f_2, \ldots, f_{Q-1})^\dagger$: the (column) vector of distribution functions at $\boldsymbol{r}_j$ and t_n, and Q is the number of discrete velocities
- J_m: the mth-order Bessel function of the first kind
- L: characteristic length
- LBE: lattice Boltzmann equation
- LGSEM: Legendre–Galerkin spectral element method
- m_i, $0 \le i \le Q-1$: the velocity moments in the LBE
- $\mathbf{m}(\boldsymbol{r}_j, t_n) := (m_0, m_1, m_2, \ldots, m_{Q-1})^\dagger$: the (column) vector of moments at $\boldsymbol{r}_j$ and t_n
- $\mathbf{m}^{(0)}(\boldsymbol{r}_j, t_n) := (m_0^{(0)}, m_1^{(0)}, m_2^{(0)}, \ldots, m_{Q-1}^{(0)})^\dagger$: the (column) vector of equilibrium moments at $\boldsymbol{r}_j$ and t_n
- $\mathbf{M}$: the transform matrix which maps the distributions $\{f_i\}$ to the corresponding velocity moments $\{m_i\}$, *i.e.*, $\mathbf{m} = \mathbf{M}\mathbf{f}$
- $\hat{\boldsymbol{n}}$: the unit vector out-normal to the flow boundary $\partial\Omega$
- N: the number of apexes of a regular polygon
- N_{LB}: the number of fluid nodes in an LBE simulation
- N_{S}: the number nodes in one dimension for LGSEM
- p: the pressure field
- $p_{xx} = m_3$ and $p_{xy} = m_4$: the second-order moments corresponding to the diagonal and off-diagonal element of the stress tensor in 2D
- $q_x = m_6$ and $q_y = m_7$: the components of third-order moments
- $\boldsymbol{r} \in \mathbb{R}^d$: the vector (position) in d-dimensional Euclidean space
- $\boldsymbol{r}_j \in \mathbb{Z}_d$: a node on the d-dimensional lattice
- R: the radius of disc or the circum-circle of an N-polygon
- s_i $0 \le i \le Q-1$: the relaxation rates in the LBE
- s_ν and s_q: the relaxation rates corresponding to the second-order moments, m_3 and m_4, and third-order moments, m_6 and m_7
- $\mathbf{S} := \mathrm{diag}(s_0, s_1, \ldots, s_{Q-1})$: the diagonal matrix of relaxation rates
- t: time variable

- t_n: discrete time
- T: a value of time t
- $\boldsymbol{u} \in \mathbb{R}^d$: the velocity field
- $\boldsymbol{u}_0$: the initial velocity field $\boldsymbol{u}_0 := \boldsymbol{u}(\boldsymbol{r}, t = 0)$

Greek and other symbols:

- δ_t: the time step size
- δ_x: the lattice constant of the lattice in the LBE
- Δ: the Laplacian, *i.e.*, $\Delta := \boldsymbol{\nabla} \cdot \boldsymbol{\nabla}$
- $\epsilon = m_8$: the fourth-order moment
- ζ: the eigenvalue of $\mathbf{A}$
- θ: the angular variable in two-dimensional polar coordinates
- $\lambda(N)$: the Stokes eigenvalue depending on the number of apexes N
- λ_{mn}: the Stokes eigenvalue on a circular disc
- λ_*: the computed Stokes eigenvalue
- ν: the shear viscosity
- ρ: the flow mass density
- ψ: the stream function
- ψ_{mn}: the stream eigenfunction depending on the radial quantum number n and angular quantum number m
- Ω: a flow domain in $\mathbb{R}^d$
- $\partial\Omega$: the boundary of a domain Ω
- $\boldsymbol{\nabla}$: the gradient operator in d-dimensional space
- †: transpose operation

CRediT authorship contribution statement

Pierre Lallemand: Conceptulization, Methodology, Data curation, Formal analysis, Writing - original draft, Writing - review & editing. **Lizhen Chen:** Methodology, Data curation, Formal analysis, Original draft, Writing - review & editing. **Gérard Labrosse:** Conceptulization, Methodology, Data curation, Formal analysis, Writing - original draft, Writing - review & editing. **Li–Shi Luo:** Methodology, Data curation, Formal analysis, Writing - original draft, Writing - review & editing, Project administration, Funding acquisition.

Declaration of competing interest

The authors declare that they have no known competing financial interests or personal relationships that could have appeared to influence the work reported in this paper.

Acknowledgements

This work is supported by the National Natural Science Foundation of China (NSFC) under the Grants U1530401 and U1930402. The computational resources were provided by Beijing Computational Science Research Center, China (CSRC, www.csrc.ac.cn). LZC would like to acknowledge the support from NSFC through the Grant 11671166.

References

[1] Leriche E, Labrosse G. Stokes eigenmodes in square domain and the stream function-vorticity correlation. J Comput Phys 2004;200(2):489–511.
[2] Labrosse G, Leriche E, Lallemand P. Stokes Eigenmodes in cubic domain: their symmetry properties. Theor Comput Fluid Dyn 2014;28(3):335–56.
[3] Chen L, Labrosse G, Lallemand P, Luo L-S. Spectrally accurate Stokes eigen-modes on isosceles triangles. Comput Fluids 2016;136:1–9.
[4] Kelliher JP. Eigenvalues of the Stokes operator versus the Dirichlet Laplacian in the plane. Pac J Math 2010;244(1):99–132.
[5] Yolcu SY, Yolcu T. Multidimensional lower bounds for the eigenvalues of Stokes and Dirichlet Laplacian operators, J Math Phys, 0000, 53.
[6] Kac M. Can one hear the shape of a drum?. Am Math Mon 1991;73(4):641–787.
[7] Protter M. Can one hear the shape of a drum? revisited. SIAM Rev 1987;29(2):185–97. http://dx.doi.org/10.1137/1029041.
[8] Fabre J. Can one hear the shape of a drum. Recherche 1988;19(202):1104–6.
[9] Ben Amar M, da Silva P. Can one hear the shape of a smectic drum?. Proc R Soc Lond Ser A Math Phys Eng Sci 1998;454(1978):2757–65. http://dx.doi.org/10.1098/rspa.1998.0279.
[10] Okada Y, Shudo A, Tasaki S, Harayama T. 'Can one hear the shape of a drum?': revisited. J Phys A 2005;38(9):L163–70. http://dx.doi.org/10.1088/0305-4470/38/9/L02.
[11] Zuluaga S, Fonseca F. Can't one really hear the shape of a drum?. Acoust Phys 2011;57(4):465–72. http://dx.doi.org/10.1134/S106377101104021X.
[12] Courant R, Hilbert D. Methods of mathematical physics, Vol. 1. New York: Interscience Publishers, Inc.; 1953.
[13] Métivier G. Valeurs propres de problèmes aux limites elliptiques irréguliers. Mém Soc Math Fr 1977;51–52:125–219.
[14] Métivier G. Valeurs propres des opérateurs définis sur la restriction de systèmes variationnels à des sous-espaces. J Math Pures Appl 1978;57:133–56.
[15] Hörmander L. The analysis of linear partial differential operators, Vol. IV. Berlin: Springer; 1985.
[16] Lapidus ML, drum Fractal. Fractal drum inverse spectral problems for elliptic-operators and a partial resolution of the weyl-berry conjecture. Trans Amer Math Soc 1991;325(2):465–529. http://dx.doi.org/10.2307/2001638.
[17] Lapidus ML, Radunović G, Žubrinić D. Fractal zeta functions and complex dimensions of relative fractal drums. J Fixed Point Theory Appl 2014;15(2):321–78.
[18] Leriche E, Labrosse G. High-order direct Stokes solvers with or without temporal splitting: Numerical investigations of their comparative properties. SIAM J Sci Comput 2000;22(4):1386–410.
[19] Leriche E, Lallemand P, Labrosse G. Stokes eigenmodes in cubic domain: Primitive variable and lattice Boltzmann formulations. Appl Numer Math 2008;58:935–45.
[20] Leriche E, Labrosse G. Are there localized eddies in the trihedral corners of the Stokes eigenmodes in cubical cavity?. Comput Fluids 2011;43:98–101.
[21] Lallemand P, Luo LS, Krafczyk M, Yong W-A. The lattice Boltzmann method for nearly incompressible flows. J Comput Phys 2021;431:109713.
[22] d'Humières D. Generalized lattice-Boltzmann equations. In: Shizgal BD, Weave DP, editors. Rarefied gas dynamics: theory and simulations. Prog. astronaut. aeronaut., Vol. 159, Washington, D.C: AIAA; 1992, p. 450–8.
[23] d'Humières D, Ginzburg I, Krafczyk M, Lallemand P, Luo L-S. Multiple-relaxation-time lattice Boltzmann models in three-dimensions. Philos Trans R Soc Lond Ser A 2002;360(1792):437–51.
[24] Junk M, Yong W-A. Rigorous Navier–Stokes limit of the lattice Boltzmann equation. Asymptotic Anal 2003;35:165–85.
[25] Junk M, Klar A, Luo L-S. Asymptotic analysis of the lattice Boltzmann equation. J Comput Phys 2005;210(2):676–704. http://dx.doi.org/10.1016/j.jcp.2005.05.003.
[26] Dubois F. Equivalent partial differential equations of a lattice Boltzmann scheme. Comput Math Appl 2008;55(7):1441–9.
[27] Dubois F, Lallemand P. Towards higher order lattice Boltzmann schemes. J Stat Mech Theory Exp 2009;2009:P06006.
[28] Junk M, Yang Z. Convergence of lattice Boltzmann methods for Navier–Stokes flows in periodic and bounded domains. Numer Math 2009;112(1):65–87.
[29] Dubois F, Lallemand P, Tekitek M. On a superconvergent lattice Boltzmann boundary scheme. Comput Math Appl 2010;59(7):2141–9.
[30] Dubois F, Lallemand P. Quartic parameters for acoustic applications of lattice Boltzmann scheme. Comput Math Appl 2011;61(12):3404–16. http://dx.doi.org/10.1016/j.camwa.2011.01.011.
[31] Bouzidi M, Firdaouss M, Lallemand P. Momentum transfer of Boltzmann-lattice fluid with boundaries. Phys Fluids 2001;13(11):3452–9.
[32] Duffy M. Quadrature over a pyramid or cube of integrands with a singularity at a vertex. SIAM J Numer Anal 1982;19(6):1260–2.
[33] Dubiner M. Spectral methods on triangles and other domains. J Sci Comput 1991;6(4):345–90.
[34] Sherwin S, Karniadakis G. A triangular spectral element method: Applications to the incompressible Navier–Stokes equations. Comput Method Appl Mech 1995;123(1–4):189–229.
[35] Owens R. Spectral approximations on the triangle. Proc R Soc Lond Ser A Math Phys Eng Sci 1998;454(1971):857–72.
[36] Karniadakis G, Sherwin S. Spectral/Hp element methods for cfd. Oxford University Press; 1999.
[37] Braess D, Schwab C. Approximation on simplices with respect to weighted Sobolev norms. J Approx Theory 2000;103(2):329–37.
[38] Chen L, Shen J, Xu C. A triangular spectral method for the Stokes equations. Numer Math Theor Methods Appl 2011;4(2):158–79.
[39] Chen L, Shen J, Xu C. A unstructured nodal spectral-element method for the Navier–Stokes equations. Commun Comput Phys 2012;12(1):315–36.
[40] Shen J. Efficient spectral-Galerkin method part 1: Direct solvers of 2nd-order and 4th-order equations using Legendre polynomials. SIAM J Sci Comput 1994;15(6):1489–505.